change sign when one passes from one domain state to the other. Since there is no intermediate group between G and F, there are no secondary tensor parameters.

Example 3.1.3.4.2. Phase transitions in barium titanate ($BaTiO_3$). We shall illustrate the solution of the inverse Landau problem and the need to correlate the crystallographic system with the Cartesian crystallophysical coordinate system. The space-group type of the parent phase is $\mathcal{G} = Pm\bar{3}m$, and those of the three ferroic phases are $\mathcal{F}_1^{(1)} = P4mm$, $\mathcal{F}_1^{(2)} = Cm2m$, $\mathcal{F}_1^{(3)} = R3m$, all with one formula unit in the primitive unit cell.

This information is not complete. To perform mode analysis, we must specify these space groups by saying that the lattice symbol P in the first case and the lattice symbol R in the third case are given with reference to the cubic crystallographic basis (**a**, **b**, **c**), while lattice symbol C in the second case is given with reference to crystallographic basis [(**a** − **b**), (**a** + **b**), **c**]. If we now identify vectors of the cubic crystallographic basis with vectors of the Cartesian basis by $\mathbf{a} = a\mathbf{e}_x$, $\mathbf{b} = a\mathbf{e}_y$, $\mathbf{c} = a\mathbf{e}_z$, where $\mathbf{e}_x$, $\mathbf{e}_y$, $\mathbf{e}_z$ are three orthonormal vectors, we can see that the corresponding point groups are $F_1^{(1)} = 4_z m_x m_{xy}$, $F_1^{(2)} = m_{x\bar{y}} 2_{xy} m_z$, $F_1^{(3)} = 3_p m_{x\bar{y}}$.

Notice that without specification of crystallographic bases one could interpret the point group of the space group $Cm2m$ as $m_x 2_y m_z$. Bases are therefore always specified in lattices of equitranslational subgroups of the space groups that are available in the software *GI*⋆*KoBo*-1, where we can check that all three symmetry descents are equitranslational.

In Table 3.1.3.1, we find that these three ferroic subgroups are epikernels of the R-irep $\Gamma_\eta = T_{1u}$ with the following principal tensor components: P_3, $P_1 = P_2$, $P_1 = P_2 = P_3$, respectively. Other principal tensor parameters can be found in the main tables of the software *GI*⋆*KoBo*-1. The knowledge of the representation Γ_η allows one to perform soft-mode analysis (see *e.g.* Rousseau *et al.*, 1981).

For the tetragonal ferroelectric phase with $F_1 = 4_z m_x m_y$, we find in Fig. 3.1.3.1 an intermediate group $L_1 = 4_z/m_z m_x m_{xy}$. In Table 3.1.3.1, we check that this is an epikernel of the R-irep E_g with secondary tensor parameter δu_3. This phase is a full (proper) ferroelectric and partial ferroelastic one.

More details about symmetry aspects of structural phase transitions can be found in monographs by Izyumov & Syromiatnikov (1990), Kociński (1983, 1990), Landau & Lifshitz (1969), Lyubarskii (1960), Tolédano & Dmitriev (1996) and Tolédano & Tolédano (1987). Group–subgroup relations of space groups are treated extensively in *IT* A1 (2003).

3.1.4. Example of a table for non-equitranslational phase transitions

By J.-C. Tolédano

In the preceding Section 3.1.3, a systematic tabulation of possible symmetry changes was provided for the class of equitranslational phase transitions. This tabulation derives from the principles described in Section 3.1.2, and relates the enumeration of the symmetry changes at structural transitions to the characteristics of the irreducible representations of the space group $\mathcal{G}$ of the 'parent' (highest-symmetry) phase adjacent to the transition. Systematic extension of this type of tabulation to the general case of transitions involving both a decrease of translational and of point-group symmetry has been achieved by several groups (Tolédano & Tolédano, 1976, 1977, 1980, 1982; Stokes & Hatch, 1988). The reader can refer, in particular, to the latter reference for an exhaustive enumeration of the characteristics of possible transitions. An illustration of the results obtained for a restricted class of parent phases (those associated with the point symmetry $4/m$ and to a simple Bravais lattice P) is presented here.

In order to clarify the content Table 3.1.4.1, let us recall (*cf.* Section 3.1.2) that Landau's theory of continuous phase transitions shows that the order parameter of a transition transforms according to a physically irreducible representation of the space group $\mathcal{G}$ of the high-symmetry phase of the crystal. A physically irreducible representation is either a real irreducible representation of $\mathcal{G}$ or the direct sum of two complex-conjugate irreducible representations of $\mathcal{G}$. To classify the order-parameter symmetries of all possible transitions taking place between a given parent (high-symmetry) phase and another (low-symmetry) phase, it is therefore necessary, for each parent space group, to list the various relevant irreducible representations.

Each irreducible representation of a given space group can be denoted $\Gamma_n(k^*)$ and identified by two quantifies. The star k^*, represented by a vector linking the origin of reciprocal space to a point of the first Brillouin zone, specifies the translational symmetry properties of the basis functions of $\Gamma_n(k^*)$. The dimension of $\Gamma_n(k^*)$ is equal to the number of components of the order parameter of the phase transition considered. A given space group has an infinite number of irreducible representations. However, physical considerations restrict a systematic enumeration to only a few irreducible representations. The restrictions arise from the fact that one focuses on continuous (or almost continuous) transitions between strictly periodic crystal structures (*i.e.* in particular, incommensurate phases are not considered), and have been thoroughly described previously (Tolédano & Tolédano, 1987, and references therein).

3.1.5. Microscopic aspects of structural phase transitions and soft modes

By J. F. Scott

3.1.5.1. *Introduction*

Phase transitions in crystals are most sensitively detected *via* dynamic techniques. Two good examples are ultrasonic attenuation and internal friction. Unfortunately, while often exquisitely sensitive to subtle second-order phase transitions [*e.g.* the work of Spencer *et al.* (1970) on $BaMnF_4$], they provide no real structural information on the lattice distortions that occur at such phase transitions, or even convincing evidence that a real phase transition has occurred (*e.g.* transition from one long-range thermodynamically stable ordered state to another). It is not unusual for ultrasonic attenuation to reveal a dozen reproducible anomalies over a small temperature range, none of which might be a phase transition in the usual sense of the phrase. At the other extreme are detailed structural analyses *via* X-ray or neutron scattering, which give unambiguous lattice details but often totally miss small, nearly continuous rigid rotations of light ions, such as hydrogen bonds or oxygen or fluorine octahedra or tetrahedra. Intermediate between these techniques are phonon spectroscopies, notably infrared (absorption or reflection) and Raman techniques. The latter has developed remarkably over the past thirty years since the introduction of lasers and is now a standard analytical tool for helping to elucidate crystal structures and phase transitions investigated by chemists, solid-state physicists and materials scientists.

3.1.5.2. *Displacive phase transitions*

3.1.5.2.1. *Landau–Devonshire theory*

Landau (1937) developed a simple mean-field theory of phase transitions which implicitly assumes that each atom or ion in a system exerts a force on the other particles that is independent of the distance between them (see Section 3.1.2.2). Although this is a somewhat unphysical crude approximation to the actual forces, which are strongly dependent upon interparticle spacings, it allows the forces of all the other particles in the system to be replaced mathematically by an effective 'field', and for the

Copyright © 2006 International Union of Crystallography

resulting equations to be solved exactly. This mathematical simplicity preserves the qualitative features of the real physical system and its phase transition without adding unnecessary cumbersome mathematics and had earlier been used to great advantage for fluids by Van der Waals (1873) and for magnetism by Weiss (1907). Landau's theory is a kind of generalization of those earlier theories. In it he defines an 'order parameter' x, in terms of which most physical quantities of interest may be expressed *via* free energies. In a ferromagnet, the order parameter corresponds to the net magnetization; it is zero above the Curie temperature T_c and increases monotonically with decreasing temperature below that temperature. In a liquid–gas phase transition the order parameter is the difference in density in the gas and liquid phases for the fluid.

Devonshire independently developed an equivalent theory for ferroelectric crystals around 1953 (Devonshire, 1954). For ferroelectrics, the order parameter is the spontaneous dielectric polarization P. In both his formalism and that of Landau, the ideas are most conveniently expressed through the free energy of the thermodynamic system:

$$F(P, T) = A(T - T_c)P^2 + BP^4 + CP^6, \qquad (3.1.5.1a)$$

where A and C are positive quantities and B may have either sign. Scott (1999) shows that C changes sign at ferroelectric-to-superionic conducting transition temperatures. As shown in Fig. 3.1.5.1, minimization of the free energy causes the expectation value of P to go from zero above the Curie temperature to a nonzero value below. If B is positive the transition is continuous ('second-order'), whereas if B is negative, the transition is discontinuous ('first-order'), as shown in Fig. 3.1.5.2. The coefficient B may also be a function of pressure p or applied electric field **E** and may pass through zero at a critical threshold value of p or **E**. Such a point is referred to as a 'tricritical point' and is marked by a change in the order of the transition from first-order to second-order. The term '*tri*-critical' originates from the fact that in a three-dimensional graph with coordinates temperature T, pressure p and applied field **E**, there are *three* lines marking the ferroelectric–paraelectric phase boundary that meet at a single point. Crossing any of these three lines produces a continuous phase transition (Fig. 3.1.5.3).

3.1.5.2.2. *Soft modes*

Minimization of the free energy above leads to the dependence of spontaneous polarization P upon temperature given by $P(T) = P(0)[(T_c - T)/T_c]$ for continuous transitions. In the more general case discussed by Landau, the polarization P is replaced by a generic 'order parameter' $\varphi(T)$ with the same dependence. Cochran's contribution (1960, 1961) was to show that for

Table 3.1.4.1. *Possible symmetry changes across transitions from a parent phase with space group $P4/m$, $P4_2/m$, $P4/n$, $P4_2/n$, $I4/m$ or $I4_1/a$*

Equitranslational symmetry changes are not included (*cf.* Section 3.1.3). The coordinates of the points in the second column are referred to the primitive unit cell of the reciprocal lattice. The terms used in the fifth column are introduced in Section 3.1.1. The last column is characteristic of non-equitranslational transitions.

Parent space group	Irreducible representation: Brillouin zone point	Irreducible representation: Dimension of the order parameter	Possible low-symmetry space groups	Macroscopic characteristics of the transition	Change in the number of atoms per primitive unit cell
$P4/m$	$\frac{1}{2},\frac{1}{2},0$	2	$P2/m$; $P2/b$	Ferroelastic	2
		1	$P4/m$; $P4/n$	Non-ferroic	2
	$0,0,\frac{1}{2}$	2	$P2_1/m$	Ferroelastic	2
		1	$P4/m$; $P4_2/m$	Non-ferroic	2
	$\frac{1}{2},\frac{1}{2},\frac{1}{2}$	2	$B2/m$	Ferroelastic	2
		1	$I4/m$	Non-ferroic	2
	$0,\frac{1}{2},\frac{1}{2}$	2	$B2/m$	Ferroelastic	2
		1	$I4/m$	Non-ferroic	4
	$0,\frac{1}{2},0$	2	$P2/m$; $P2/b$	Ferroelastic	2
		1	$P4/m$; $P4/n$	Non-ferroic	4
$P4_2/m$	$\frac{1}{2},\frac{1}{2},0$	2	$P2/m$; $P2/b$	Ferroelastic	2
		1	$P4_2/n$; $P4_2/m$	Non-ferroic	2
	$0,0,\frac{1}{2}$	2	$P2_1/m$	Ferroelastic	2
		2	$P4_1$; $P4_3$	Ferroelectric	2
	$\frac{1}{2},\frac{1}{2},\frac{1}{2}$	2	$B2/m$	Ferroelastic	2
		1	$I4/m$	Non-ferroic	2
	$0,\frac{1}{2},\frac{1}{2}$	2	$B2/m$	Ferroelastic	2
		2	$P4_1/a$	Non-ferroic	2
	$0,\frac{1}{2},0$	2	$P2/m$; $P2/b$	Ferroelastic	2
		2	$P4_2/m$; $P4_2/n$	Non-ferroic	2
$P4/n$	$\frac{1}{2},\frac{1}{2},0$	2	$P2/b$	Ferroelastic	2
		2	$P4$	Ferroelectric	2
	$0,0,\frac{1}{2}$	2	$P2_1/b$	Ferroelastic	2
		1	$P4/n$; $P4_2/n$	Non-ferroic	2
	$\frac{1}{2},\frac{1}{2},\frac{1}{2}$	2	$B2/b$	Ferroelastic	2
		2	$I4$	Ferroelectric	2
$P4_2/n$	$\frac{1}{2},\frac{1}{2},0$	2	$P2/b$	Ferroelastic	2
	$0,0,\frac{1}{2}$	2	$P2_1/b$	Ferroelastic	2
		2	$P4_1$; $P4_3$	Ferroelectric	2
$I4/m$	$\frac{1}{2},-\frac{1}{2},-\frac{1}{2}$	2	$P2_1/m$; $P2_1/b$	Ferroelastic	2
		1	$P4/m$; $P4_2/m$; $P4/n$; $P4_2/n$	Non-ferroic	2
	$\frac{1}{2},\frac{1}{2},0$	2	$B2/m$; $B2/b$	Ferroelastic	2
		2	$P4/m$; $P4_2/m$; $P4/n$; $P4_2/n$	Non-ferroic	4
	$\frac{1}{2},0,0$	4	$B2/m$	Ferroelastic	2
		4	$P\bar{1}$	Ferroelastic	8
		4	$I4/m$; $I4_1/a$	Non-ferroic	8
	$\frac{3}{4},\frac{1}{4},-\frac{1}{4}$	2	$I4/m$; $I4_1/a$	Non-ferroic	4
$I4_1/a$	$\frac{1}{2},-\frac{1}{2},-\frac{1}{2}$	2	$P2_1/b$	Ferroelastic	2
	$\frac{1}{2},0,0$	4	$I\bar{4}$	Higher-order ferroic	8
		4	$P\bar{1}$	Ferroelastic	2
		4	$P\bar{1}$; $B2/b$	Ferroelastic	4

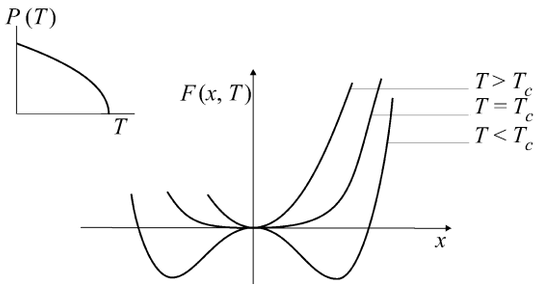

Fig. 3.1.5.1. Free energy $F(P, T)$ and order parameter $P(T)$ from the Landau–Devonshire theory [equation (3.1.5.1*a*)] for a continuous second-order ferroelectric phase transition [coefficient B positive in equation (3.1.5.1*a*)]. The insert shows the temperature dependence of the order parameter, *i.e.* the expectation value of the displacement $x(T)$.

continuous 'displacive' (as opposed to 'order–disorder') transitions, this order parameter is (or is proportional to) a normal mode of the lattice. One normal mode of the crystal must, in Cochran's theory, literally soften: the generalized force constant for this mode weakens as a function of temperature, and its frequency consequently decreases. This soft-mode theory provided an important step from the macroscopic description of Landau and Devonshire to a microscopic theory, and in particular, to vibrational (phonon) spectroscopy.

Cochran illustrated this theory using a 'shell' model in which the electrons surrounding an ion were approximated by a rigid sphere; shell–shell force constants were treated as well as shell–core and core–core terms, in the general case. The initial application was to PbTe and other rock-salt cubic structures that undergo ferroelectric structural distortions.

For this simple case, the key equations relate the optical phonon frequencies of long wavelength to two terms: a short-range force constant R'_0 and a long-range Coulombic term. It is important that in general neither of these terms has a pathological temperature dependence; in particular, neither vanishes at the Curie temperature. Rather it is the subtle cancellation of the two terms at T_c that produces a 'soft' transverse optical phonon.

The longitudinal optical phonon frequency $\omega_{\rm LO}(T)$ is positive definite and remains finite at all temperatures:

$$\mu\omega_{\rm LO}^2 = R'_0 + \frac{8\pi Z^2 e^2}{9\varepsilon V(T)}, \qquad (3.1.5.1b)$$

where μ is a reduced mass for the normal mode; Ze is an effective charge for the mode, related to the valence state of the ions involved; ε is the high-frequency dielectric constant and $V(T)$ is the unit-cell volume, which is a function of temperature due to thermal expansion.

By comparison, the transverse optical phonon frequency

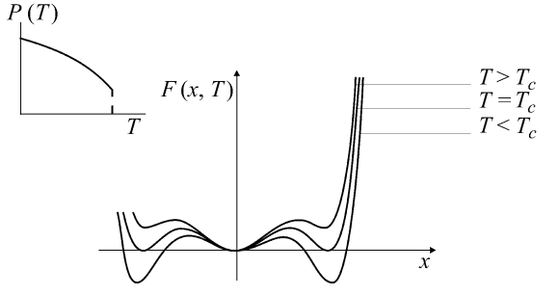

Fig. 3.1.5.2. Free energy $F(P, T)$ and order parameter $P(T)$ from the Landau–Devonshire theory [equation (3.1.5.1*a*)] for a discontinuous first-order ferroelectric phase transition [coefficient B negative in equation (3.1.5.1*a*)]. T_1 is the temperature (see Fig. 3.1.2.6) below which a secondary minimum appears in the free energy.

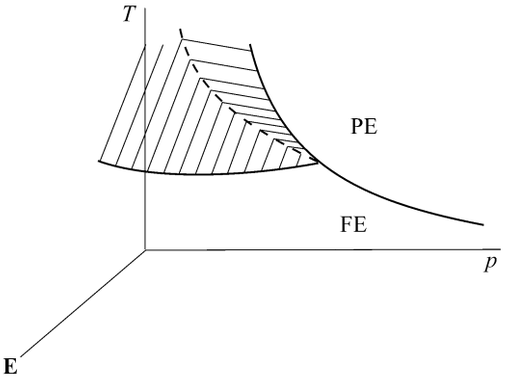

Fig. 3.1.5.3. Three-dimensional graph of phase boundaries as functions of temperature T, pressure p and applied electric field $\mathbf{E}$, showing a tricritical point where three continuous phase boundaries intersect.

$$\mu\omega_{\rm TO}^2 = R'_0 - \frac{4\pi Z^2 e^2}{3\varepsilon V(T)} \qquad (3.1.5.1c)$$

can vanish accidentally when $V(T)$ reaches a value that permits cancellation of the two terms. Note that this does not require any unusual temperature dependence of the short-range interaction term R'_0. This description appears to satisfy all well studied ferroelectrics except for the 'ultra-weak' ones epitomized by TSCC (tris-sarcosine calcium chloride), in which the Coulombic term in (3.1.5.1*b*) and (3.1.5.1*c*) is very small and the pathological dependence occurs in R'_0. This leads to a situation in which the longitudinal optical phonon is nearly as soft as is the transverse branch.

Subsequent to Cochran's shell-model developments, Cowley (1962, 1964, 1970) replaced this phenomenological modelling with a comprehensive many-body theory of phonon anharmonicity, in which the soft-mode temperature is dominated by Feynman diagrams emphasizing renormalization of phonon self-energies due to four-phonon interactions (two in and two out). This contrasts with the three-phonon interactions that dominate phonon linewidths under most conditions.

It is worth noting that the soft optical phonon branch is necessarily always observable in the low-symmetry phase *via* Raman spectroscopy in all 32 point-group symmetries. This was first proved by Worlock (1971), later developed in more detail by Pick (1969) and follows group-theoretically from the fact that the vibration may be regarded as a dynamic distortion of symmetry Γ_i which condenses at T_c to produce a static distortion of the same symmetry. Hence the vibration in the distorted phase has symmetry given by the product $\Gamma_i \times \Gamma_i$, which always contains the totally symmetric representation Γ_1 for any choice of Γ_i. If Γ_i is non-degenerate, its outer product with itself will contain only Γ_1 and there will be a single, totally symmetric soft mode; if Γ_i is degenerate, there will be two or three soft modes of different symmetries, at least one of which is totally symmetric.

Since the totally symmetric representation is Raman-active for all 32 point-group symmetries, this implies that the soft mode is always accessible to Raman spectroscopy at least in the distorted, low-symmetry phase of the crystal.

3.1.5.2.3. *Strontium titanate, $SrTiO_3$*

Among the perovskite oxides that are ferroelectric insulators, barium titanate has received by far the most attention from the scientific community since its independent characterization in several countries during World War II. The discovery of a ferroelectric that was robust, relatively inert (not water-soluble) and without hydrogen bonding was a scientific breakthrough, and its large values of dielectric constant and especially spontaneous polarization are highly attractive for devices. Although not ferroelectric in pure bulk form, strontium titanate has received

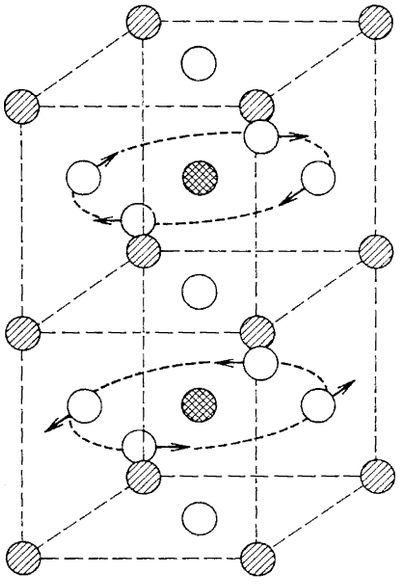

Fig. 3.1.5.4. Structure of strontium titanate above (undisplaced ions) and below (arrows) its anti-ferrodistortive phase transition at *ca.* 105 K. Below this temperature, the cubic primitive cell undergoes a tetragonal distortion and also doubles along the [001] cubic axis (domains will form along [100], [010] and [001] of the original cubic lattice). The ionic displacements approximate a rigid rotation of oxygen octahedra, out-of-phase in adjacent unit cells, except that the oxygens actually remain on the cube faces, so that a very small Ti—O bond elongation occurs.

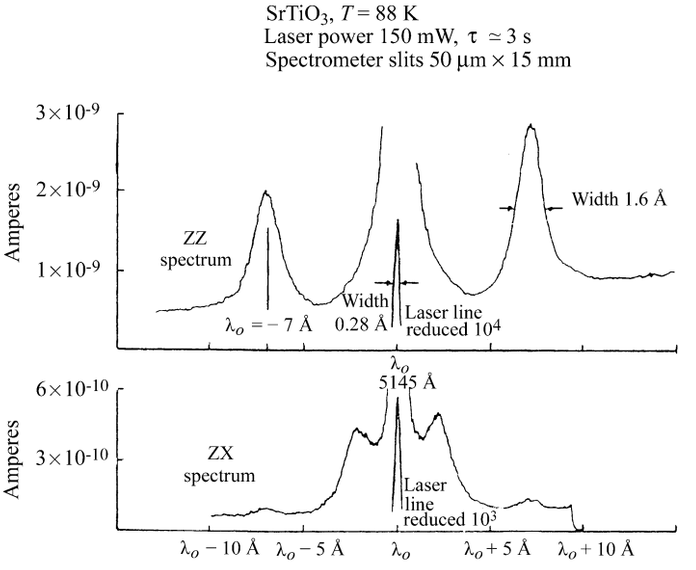

Fig. 3.1.5.6. Raman spectra of strontium titanate below its cubic–tetragonal phase transition temperature. These features disappear totally above the phase transition temperature, thereby providing a vivid indication of a rather subtle phase transition.

the second greatest amount of attention of this family over the past thirty years. It also provides a textbook example of how optical spectroscopy can complement traditional X-ray crystallographic techniques for structural determination.

Fig. 3.1.5.4 shows the structure of strontium titanate above and below the temperature ($T_0 = 105$ K) of a non-ferroelectric phase transition. Note that there is an out-of-phase distortion of oxygen ions in adjacent primitive unit cells (referred to the single formula group ABO_3 in the high-temperature phase). This out-of-phase displacement approximates a rigid rotation of oxygen octahedra about a [100], [010] or [001] cube axis, except that the oxygens actually remain in the plane of the cube faces. We note three qualitative aspects of this distortion: Firstly, it doubles the primitive unit cell from one formula group to two; this will approximately double the number of optical phonons of very long wavelength ($q = 0$) permitted in infrared and/or Raman spectroscopy. Secondly, it makes the gross crystal class tetragonal, rather than cubic (although in specimens cooled through the transition temperature in the absence of external stress, we might expect a random collection of domains with tetragonal axes along the original [100], [010], [001] cube axes, which will give macroscopic cubic properties to the multidomain aggregate). Thirdly, the transition is perfectly continuous, as shown in Fig. 3.1.5.5, where the rotation angle of the oxygen octahedra about the cube axis is plotted *versus* temperature.

Fig. 3.1.5.4 does not correspond at all to the structure inferred earlier from X-ray crystallographic techniques (Lytle, 1964). The very small, nearly rigid rotation of light ions (oxygens) in multidomain specimens caused the X-ray study to overlook the primary characteristic of the phase transition and to register instead only the unmistakable change in the c/a ratio from unity. Thus, the X-ray study correctly inferred the cubic–tetragonal characteristic of the phase transition but it got both the space

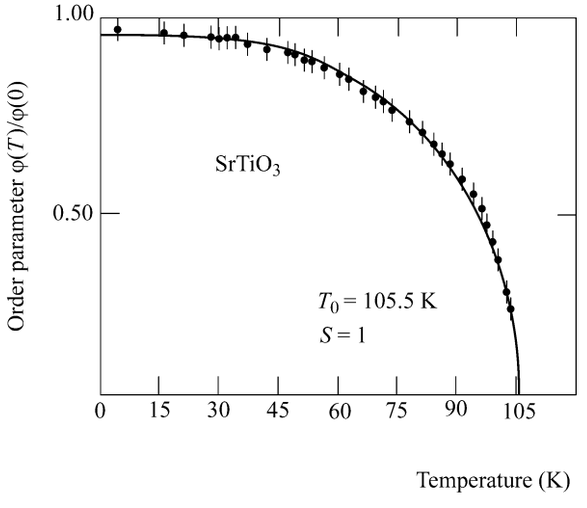

Fig. 3.1.5.5. Rotation angle *versus* temperature for the oxygen octahedron distortion below 105 K in strontium titanate described in Fig. 3.1.5.4. The solid curve is a mean-field least-squares fit to an $S = 1$ Brillouin function.

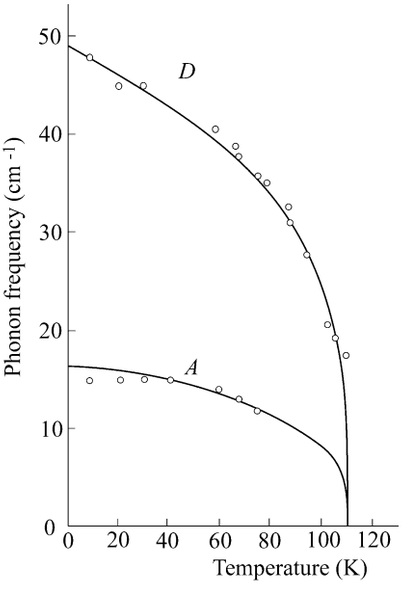

Fig. 3.1.5.7. Temperature dependence of phonon branches observed in the Raman spectra of tetragonal strontium titanate.

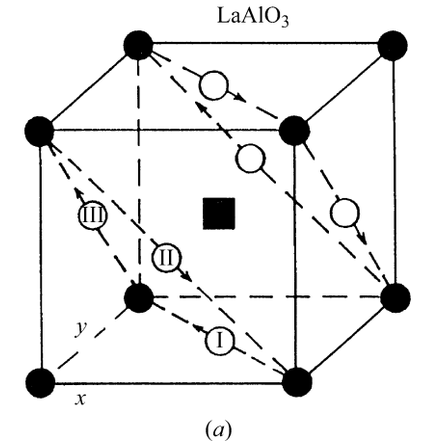

(*a*)

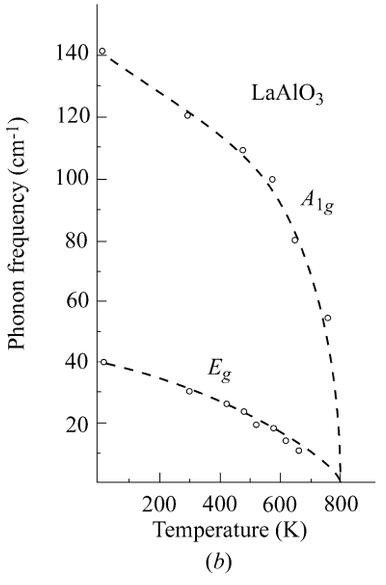

(*b*)

Fig. 3.1.5.8. (*a*) Structure of lanthanum aluminate above (undistorted) and below (arrows) its cubic–rhombohedral phase transition near 840 K. As in strontium titanate (Figs. 3.1.5.4–3.1.5.7), there is a nearly rigid rotation of oxygen octahedra (the oxygen ions actually remain on the cube faces); however, in the lanthanide aluminates (Ln = La, Pr, Nd) the rotation is about a cube [111] body diagonal, so that the resulting structure is rhombohedral, rather than tetragonal. The primitive unit cell doubles along the cubic [111] axis; domains will form with the unique axis along all originally equivalent body diagonals of the cubic lattice. (*b*) Optical phonon frequences *versus* temperature in lanthanum aluminate.

group and the size of the primitive cell wrong. The latter error has many serious implications for solid-state physicists: For example, certain electronic transitions from valence to conduction bands are actually 'direct' (involving no change in wavevector) but would have erroneously been described as 'indirect' with the structure proposed by Lytle. More serious errors of interpretation arose with the microscopic mechanisms of ultrasonic loss proposed by Cowley based upon Lytle's erroneous structure.

The determination of the correct structure of strontium titanate (Fig. 3.1.5.4) was actually made *via* EPR studies (Unoki & Sakudo, 1967) and confirmed *via* Raman spectroscopy (Fleury *et al.*, 1968). The presence of 'extra' $q = 0$ optical phonon peaks in the Raman spectra below T_0 (Fig. 3.1.5.6) is simple and unmistakable evidence of unit-cell multiplication. The fact that two optical phonon branches have frequencies that decrease continuously to zero (Fig. 3.1.5.7) as the transition temperature is approached from below shows further that the transition is 'displacive', that is, that the structures are perfectly ordered both above and below the transition temperature. This is a classic example of Cochran's soft-mode theory discussed above.

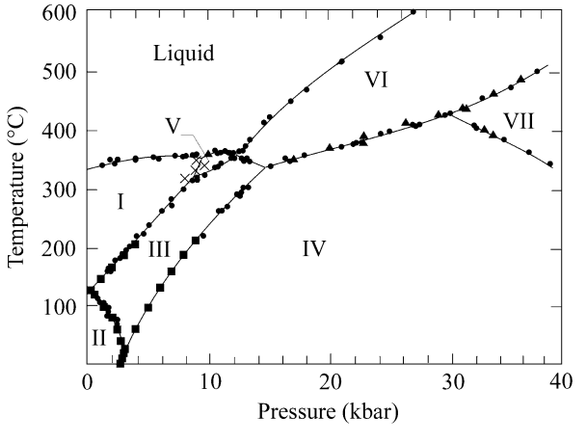

Fig. 3.1.5.9. Phase diagram of potassium nitrate, KNO_3.

3.1.5.2.4. *Lanthanum aluminate, $LaAlO_3$*

A structural distortion related to that in strontium titanate is exhibited in lanthanum aluminate at approximately 840 K. As in strontium titanate, the distortion consists primarily of a nearly rigid rotation of oxygen octahedra. However, in the lanthanide aluminates (including $NdAlO_3$ and $PrAlO_3$) the rotation is about the [111] body diagonal(s) of the prototype cubic structure. The rotation, shown in Fig. 3.1.5.8, is out-of-phase in adjacent cubic unit cells, analogous to that in strontium titanate.

Historically, this phase transition and indeed the structure of lanthanum aluminate were incorrectly characterized by X-ray crystallography (Geller & Bala, 1956) and correctly assigned by Scott (1969) and Scott & Remeika (1970) *via* Raman spectroscopy. The causes were as in the case of strontium titanate, namely that it is difficult to assess small, nearly rigid rotations of light ions in twinned specimens. In the case of lanthanum aluminate, Geller and Bala incorrectly determined the space group to be $R\bar{3}m$ (D^5_{3d}), rather than the correct $R\bar{3}2/c$ (D^6_{3d}) shown in Fig. 3.1.5.8, and they had the size of the primitive unit cell as one formula group rather than two.

3.1.5.2.5. *Potassium nitrate, KNO_3*

Potassium nitrate has a rather simple phase diagram, reproduced in Fig. 3.1.5.9. Two different structures and space groups were proposed for the ambient temperature phase I: Shinnaka (1962) proposed D^6_{3d} ($R\bar{3}2/c$) with two formula groups per primitive cell ($Z = 2$), whereas Tahvonen (1947) proposed D^5_{3d} ($R\bar{3}m$) with one formula group per primitive cell. In fact, both are wrong. The correct space group is that of Nimmo & Lucas (1973): D^6_{3d} ($R\bar{3}2/c$) with one formula group per primitive cell. Again, Raman spectroscopy of phonons shows that the Tahvonen structure predicts approximately twice as many spectral lines as can be observed. Balkanski *et al.* (1969) tried creatively but unsuccessfully to account for their spectra in terms of Tahvonen's space-group symmetry assignment for this crystal; later Scott & Pouligny (1988) showed that all spectra were compatible with the symmetry assigned by Nimmo and Lucas. In this case, in contrast to the perovskites strontium titanate and lanthanum aluminate, the confusion regarding space-group symmetry arose from the large degree of structural disorder found in phase I of KNO_3. The structures of phases II and III are unambiguous and are, respectively, aragonite D^{16}_{2h} (*Pnma*) with $Z = 4$ and C^5_{3v} ($R3m$) with $Z = 1$.

3.1.5.2.6. *Lanthanum pentaphosphate*

The lanthanide pentaphosphates (La, Pr, Nd and TbP_5O_{14}) consist of linked ribbons of PO_4 tetrahedra. In each material a structural phase transition occurs from a high-temperature D^7_{2h} (*Pncm*) point-group symmetry orthorhombic phase to a C_{2h}

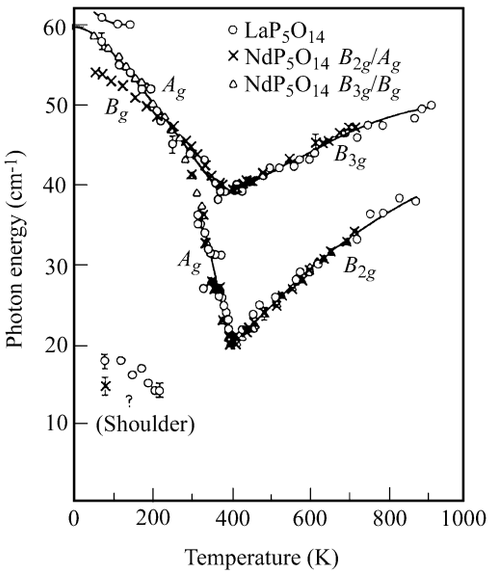

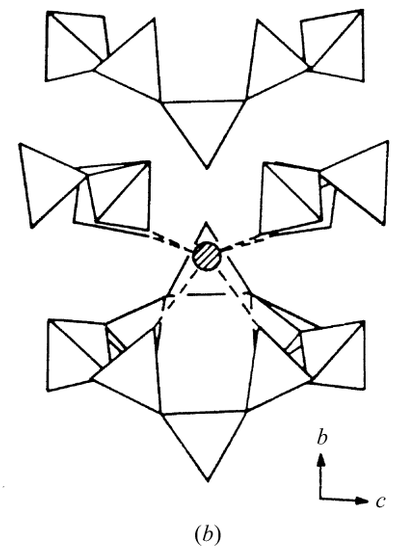

Fig. 3.1.5.10. (*a*) 'Soft' optical phonon frequency *versus* temperature in LaP_5O_{14}, showing displacive character of the phase transition. Large acousto-optic interaction prevents the optical phonon frequency from reaching zero at the transition temperature, despite the second-order character of the transition. (*b*) Lanthanum pentaphosphate structure, showing linked 'ribbons' of phosphate tetrahedra.

($P2_1/c$) monoclinic phase. The macroscopic order parameter for this transition is simply the monoclinic angle φ, or more precisely ($\varphi - 90^\circ$). In this family of materials, the X-ray crystallography was unambiguous in its determination of space-group symmetries and required no complementary optical information. However, the Raman studies (Fox *et al.*, 1976) provided two useful pieces of structural information. First, as shown in Fig. 3.1.5.10, they showed that the phase transition is entirely displacive, with no disorder in the high-symmetry phase; second, they showed that there is a microscopic order parameter that in mean field is proportional to the frequency of a 'soft' optical phonon of long wavelength ($q = 0$). This microscopic order parameter is in fact the eigenvector of that soft mode (normal coordinate), which approximates a rigid rotation of phosphate tetrahedra.

3.1.5.2.7. *Barium manganese tetrafluoride*

$BaMnF_4$ is an unusual material whose room-temperature structure is illustrated in Fig. 3.1.5.11(*a*). It consists of MnF_6 octahedra, linked by two shared corners along the polar *a* axis,

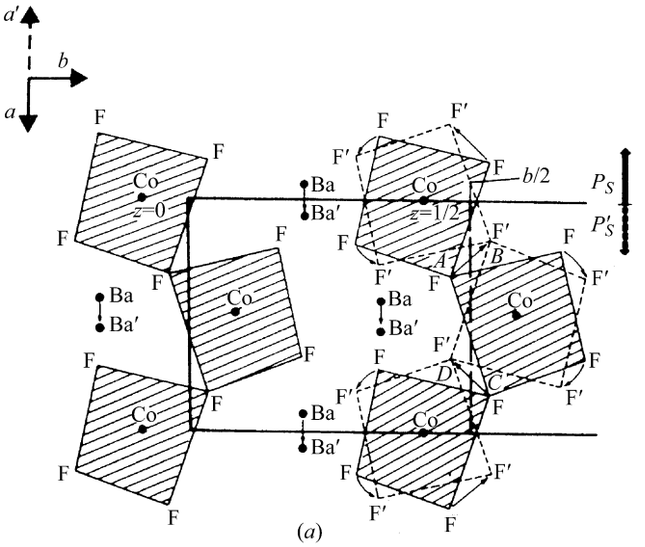

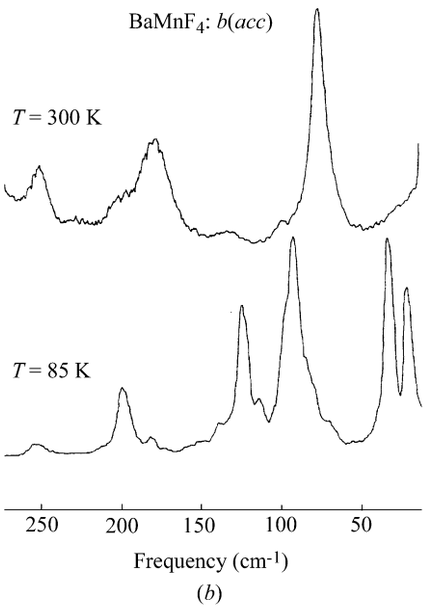

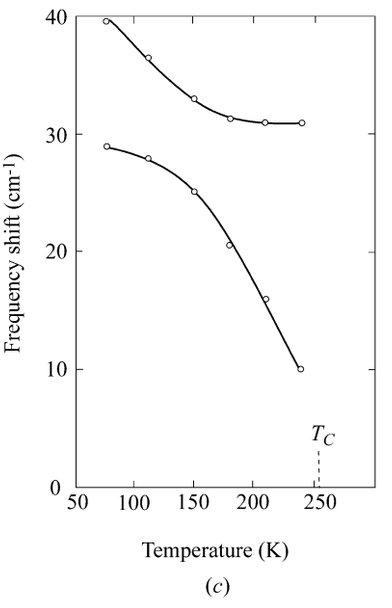

Fig. 3.1.5.11. (*a*) Structure of barium metal fluoride BaMF$_4$ (M = Co, Mn, Mg, Zn, Ni) at ambient temperature (300 K). (*b*) Raman spectroscopy of barium manganese fluoride above and below its structural phase transition temperature, *ca.* 251 K. (*c*) Temperature dependence of lower energy phonons in (*b*).

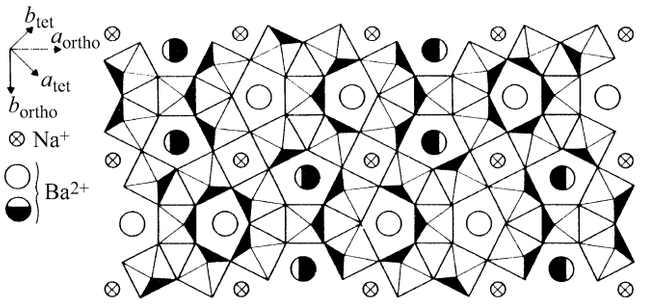

Fig. 3.1.5.12. Structure of the tungsten bronze barium sodium niobate $Ba_2NaNb_5O_{15}$ in its highest-temperature $P4/mbm$ phase above 853 K.

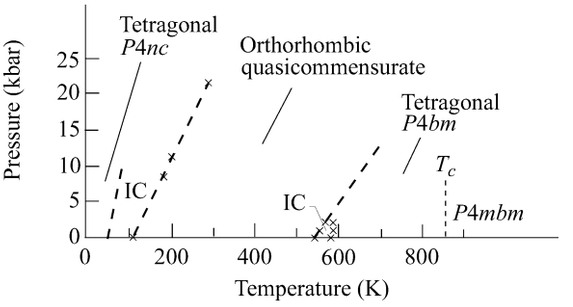

Fig. 3.1.5.13. Sequence of phases encountered with raising or lowering the temperature in barium sodium niobate.

with ribbons of such octahedra rather widely separated by the large ionic radius barium ions in the *b* direction. The resulting structure is, both magnetically and mechanically, rather two-dimensional, with easy cleavage perpendicular to the *b* axis and highly anisotropic electrical (ionic) conduction.

Most members of the BaMF$_4$ family (M = Mg, Zn, Mn, Co, Ni, Fe) have the same structure, which is that of orthorhombic C_{2v} (2*mm*) point-group symmetry. These materials are all ferroelectric (or at least pyroelectric; high conductivity of some makes switching difficult to demonstrate) at all temperatures, with an 'incipient' ferroelectric Curie temperature extrapolated from various physical parameters (dielectric constant, spontaneous polarization *etc.*) to lie 100 K or more above the melting point (*ca.* 1050 K). The Mn compound is unique in having a low-temperature phase transition. The reason is that Mn^{+2} represents (Shannon & Prewitt, 1969) an end point in ionic size (largest) for the divalent transition metal ions Mn, Zn, Mg, Fe, Ni, Co; hence, the Mn ion and the space for it in the lattice are not a good match. This size mismatch can be accommodated by the r.m.s. thermal motion above room temperature, but at lower temperatures a structural distortion must occur.

This phase transition was first detected (Spencer *et al.*, 1970) *via* ultrasonic attenuation as an anomaly near 255 K. This experimental technique is without question one of the most sensitive in discovering phase transitions, but unfortunately it gives no direct information about structure and often it signals something that is not in fact a true phase transition (in $BaMnF_4$ Spencer *et al.* emphasized that they could find no other evidence that a phase transition occurred).

Raman spectroscopy was clearer (Fig. 3.1.5.11*b*), showing unambiguously additional vibrational spectra that arise from a doubling of the primitive unit cell. This was afterwards confirmed directly by X-ray crystallography at the Clarendon Laboratory, Oxford, by Wondre (1977), who observed superlattice lines indicative of cell doubling in the *bc* plane.

The real structural distortion near 250 K in this material is even more complicated, however. Inelastic neutron scattering at Brookhaven by Shapiro *et al.* (1976) demonstrated convincingly that the 'soft' optical phonon lies not at $(0, 1/2, 1/2)$ in the Brillouin zone, as would have been expected for the *bc*-plane cell doubling suggested on the basis of Raman studies, but at $(0.39, 1/2, 1/2)$. This implies that the actual structural distortion from the high-temperature C_{2v}^{12} ($Cmc2_1$) symmetry does indeed double the primitive cell along the *bc* diagonal but in addition modulates the lattice along the *a* axis with a resulting repeat length that is incommensurate with the original (high-temperature) lattice constant *a*. The structural distortion microscopically approximates a rigid fluorine octahedra rotation, as might be expected. Hence, the chronological history of developments for this material is that X-ray crystallography gave the correct lattice structure at room temperature; ultrasonic attenuation revealed a possible phase transition near 250 K; Raman spectroscopy confirmed the transition and implied that it involved primitive cell doubling; X-ray crystallography confirmed directly the cell doubling; and finally neutron scattering revealed an unexpected incommensurate modulation as well. This interplay of experimental techniques provides a rather good model as exemplary for the field. For most materials, EPR would also play an important role in the likely scenarios; however, the short relaxation times for Mn ions made magnetic resonance of relatively little utility in this example.

3.1.5.2.8. *Barium sodium niobate*

The tungsten bronzes represented by $Ba_2NaNb_5O_{15}$ have complicated sequences of structural phase transitions. The structure is shown in Fig. 3.1.5.12 and, viewed along the polar axis, consists of triangular, square and pentagonal spaces that may or may not be filled with ions. In barium sodium niobate, the pentagonal channels are filled with Ba ions, the square channels are filled with sodium ions, and the triangular areas are empty.

The sequence of phases is shown in Fig. 3.1.5.13. At high temperatures (above $T_c = 853$ K) the crystal is tetragonal and paraelectric ($P4/mbm = D_{4h}^5$). When cooled below 853 K it becomes ferroelectric and of space group $P4bm = C_{4v}^2$ (still tetragonal). Between *ca.* 543 and 582 K it undergoes an incommensurate distortion. From 543 to *ca.* 560 K it is orthorhombic and has a '1q' modulation along a single orthorhombic axis. From 560 to 582 K it has a 'tweed' structure reminiscent of metallic lattices; it is still microscopically orthorhombic but has a short-range modulated order along a second orthorhombic direction and simultaneous short-range modulated order along an orthogonal axis, giving it an incompletely developed '2q' structure.

As the temperature is lowered still further, the lattice becomes orthorhombic but not incommensurate from 105–546 K; below 105 K it is incommensurate again, but with a microstructure quite different from that at 543–582 K. Finally, below *ca.* 40 K it becomes macroscopically tetragonal again, with probable space-group symmetry $P4nc$ (C_{4v}^6) and a primitive unit cell that is four times that of the high-temperature tetragonal phases above 582 K.

This sequence of phase transitions involves rather subtle distortions that are in most cases continuous or nearly continuous. Their elucidation has required a combination of experimental techniques, emphasizing optical birefringence (Schneck, 1982), Brillouin spectroscopy (Oliver, 1990; Schneck *et al.*, 1977; Tolédano *et al.*, 1986; Errandonea *et al.*, 1984), X-ray scattering, electron microscopy and Raman spectroscopy (Shawabkeh & Scott, 1991), among others. As with the other examples described in this chapter, it would have been difficult and perhaps impossible to establish the sequence of structures *via* X-ray techniques alone. In most cases, the distortions are very small and involve essentially only the oxygen ions.

3.1.5.2.9. *Tris-sarcosine calcium chloride (TSCC)*

Tris-sarcosine calcium chloride has the structure shown in Fig. 3.1.5.14. It consists of sarcosine molecules of formula

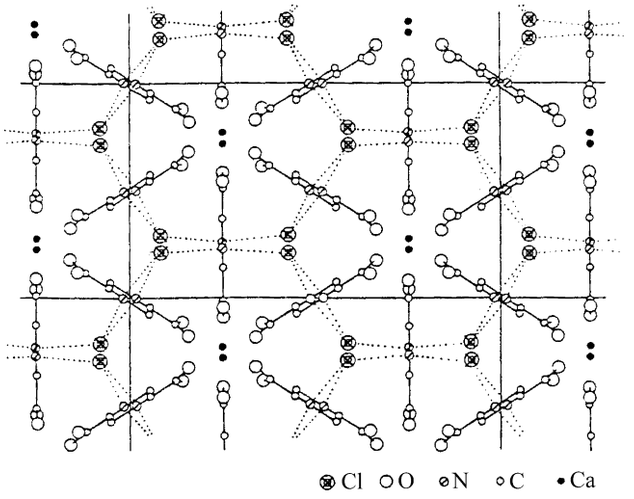

Fig. 3.1.5.14. Structure of tris-sarcosine calcium chloride, $(CH_3NHCH_2COOH)_3CaCl_2$. The hydrogen ion (proton) on the COOH group is relocated in the crystal onto the N atom to form a zwitter ion, forming an H—N—H group that hydrogen bonds to adjacent chlorine ions. Each nitrogen forms two such hydrogen bonds, whereas each chlorine has three, forming a very complex network of hydrogen bonding. The phase transition is actually displacive, involving a rather rigid rolling of whole sarcosine molecules, which stretches the N—H bonds; it is not order–disorder of hydrogen ions in a Cl···H—N double well. (The Cl···H—N wells are apparently too asymmetric for that.)

CH_3NHCH_2COOH in which the hydrogen ion comes off the COOH group and is used to hydrogen bond the nitrogen ion to a nearby chlorine, forming a zwitter ion. As is illustrated in this figure, this results in a relatively complex network of N—H···Cl bonds. The COO^- ion that results at the end group of each sarcosine is ionically bonded to adjacent calcium ions. The resulting structure is highly ionic in character and not at all that of a 'molecular crystal'. The structure at ambient temperatures is *Pnma* (D_{2h}^{16}) with $Z = 4$; below 127 K it distorts to *Pna*2$_1$ (C_{2v}^{9}) with Z still 4.

It had been supposed for some years on the basis of NMR studies of the Cl ions, as well as the conventional wisdom that 'hydrogen-bonded crystals exhibit order–disorder phase transitions', that the kinetics of ferroelectricity at the Curie temperature of 127 K in TSCC involved disorder in the proton positions along the N—H···Cl hydrogen bonds. In fact that is not correct; even the NMR data of Windsch & Volkel (1980), originally interpreted as order–disorder, actually show (Blinc *et al.*, 1970) a continuous, displacive evolution of the H-atom position along the H···Cl bond with temperature, rather than a statistical averaging

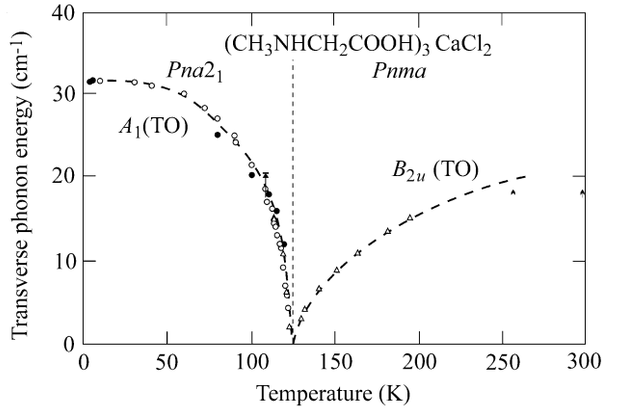

Fig. 3.1.5.15. 'Soft' optical phonon frequencies *versus* temperature in both ferroelectric and paraelectric phases of tris-sarcosine calcium chloride.

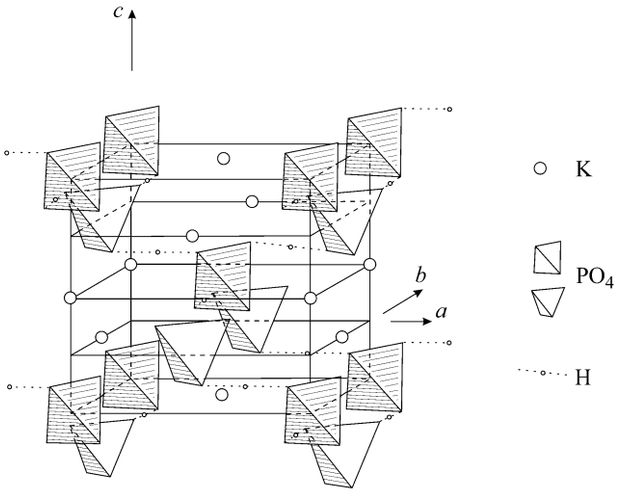

Fig. 3.1.5.16. The structure of potassium dihydrogen phosphate, KH_2PO_4, showing the O···H···O hydrogen bonds.

of two positions, which would characterize order–disorder dynamics. In addition, as shown in Fig. 3.1.5.15, there is (Kozlov *et al.*, 1983) a lightly damped 'soft' phonon branch in both the paraelectric and ferroelectric phases. TSCC is in fact a textbook example of a displacive ferroelectric phase transition. The hydrogen bonds do not exhibit disorder in the paraelectric phase. Rather, the transition approximates a rigid rotation of the sarcosine molecules, which stretches the N—H···Cl bond somewhat (Prokhorova *et al.*, 1980).

3.1.5.2.10. *Potassium dihydrogen phosphate, KH_2PO_4*

Potassium dihydrogen phosphate, colloquially termed 'KDP', has probably been the second most studied ferroelectric after barium titanate. It has been of some practical importance, and the relationship between its hydrogen bonds, shown in Fig. 3.1.5.16, the perpendicular displacement of heavier ions (K and P) and the Curie temperature has fascinated theoretical physicists, who generally employ a 'pseudo-spin model' in which the right and left displacements of the hydrogen ions along symmetric hydrogen bonds (O···H···O) can be described by a fictitious spin with up (+1/2) and down (−1/2) states.

Unlike TSCC, discussed above, KDP has perfectly symmetric hydrogen bonds. Therefore, one might expect that above a sufficiently high temperature the protons can quantum-mechanically tunnel between equivalent potential wells separated by a shallow (and temperature-dependent) barrier. Below T_C the protons order (all to the right or all to the left) in spatial regions that represent ferroelectric domains. This model, initially proposed by Blinc (1960), is correct and accounts for the large isotope shift in the Curie temperature noted for deuterated specimens. The complication is that the spontaneous polarization arises along a direction perpendicular to these proton displacements, so the dipoles do not arise from proton displacements directly. Instead, the proton coupling (largely Coulombic) to the potassium and phosphorus ions causes their displacements along the polar axis. This intricate coupling between protons along hydrogen bonds, which undergo an order–disorder transition, and K and P ions, which undergo purely displacive movements in their equilibrium positions, forms the basis of the theoretical interest in the lattice dynamics of KDP. Following Strukov & Levanyuk (1998), we would say that arguments over whether this transition is displacive or order–disorder are largely semantic; the correct description of KDP is that the thermal change in occupancy of the O···H···O double wells modifies the free energy in such a way that the K and P ions undergo a displacive rearrangement.

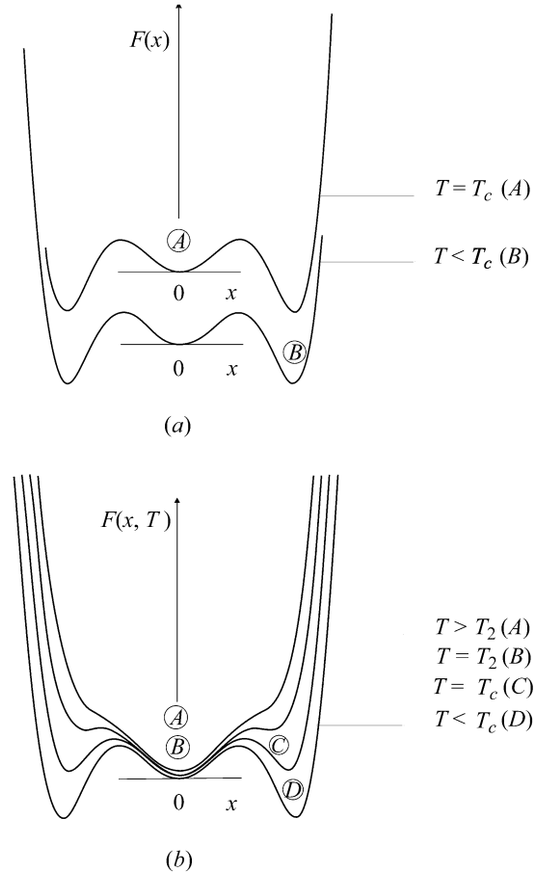

Fig. 3.1.5.17. Double-well models [circled letters show the time-averaged expectation values of the position $x(T)$ of the order parameter at each temperature]. (*a*) For purely order–disorder systems, the depth and separation of the wells is temperature-independent; only the thermal populations change, due to either true quantum-mechanical tunnelling (which only occurs for H or D ions) or thermally activated hopping (for heavier ions). (*b*) For purely displacive systems, all the temperature dependence is in the relative depths of the potential wells. [For mixed systems, such as KH_2PO_4, both well depth(s) and thermal populations change with temperature.]

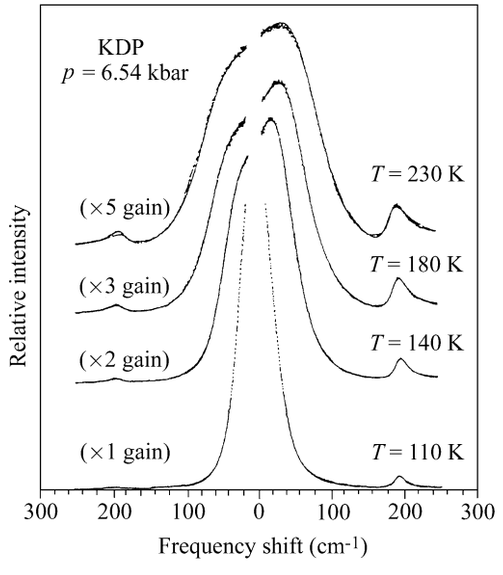

Fig. 3.1.5.18. Pressure dependence of the 'soft' optical phonon branch Raman spectra in potassium dihydrogen phosphate (after Peercy, 1975*b*), showing the displacive character of the phase transition [purely order–disorder phase transitions cannot exhibit propagating (underdamped) soft modes].

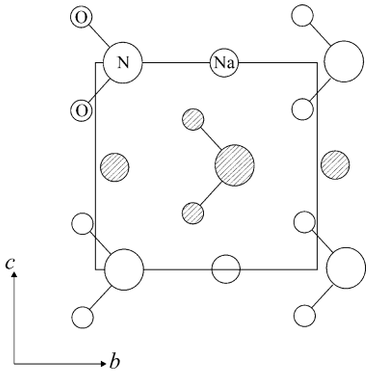

Fig. 3.1.5.19. Structure of sodium nitrite, $NaNO_2$. The molecularly bonded NO_2 ions are shaped like little boomerangs. At high temperatures they are randomly oriented, pointing up or down along the polar b axis. At low temperatures they are (almost) all pointed in the same direction ($+b$ or $-b$ domains). Over a small range of intermediate temperatures their directions have a wave-like 'incommensurate' modulation with a repeat length L that is not an integral multiple of the lattice constant b.

The difficulty comes in recognizing that the normal-mode coordinate x corresponding to the soft mode in this case involves protons (H ions) and K and P ions. Therefore, the free-energy description (as in Fig. 3.1.5.17) will have partly displacive character and partly order–disorder. If the transition were purely displacive (as in TSCC, discussed above), all the important temperature changes would be in the shape of the free energy $F(x)$ with temperature T. Whereas if the transition were purely order–disorder (as in $NaNO_2$, discussed below), the shape of the free-energy curves $F(x)$ would be quite independent of T; only the relative populations of the two sides of the double well would be T-dependent. KDP is intermediate between these descriptions. Strictly, it is 'displacive' in the sense that its normal mode is a propagating mode, shown in Fig. 3.1.5.18 by Peercy's pressure-dependence Raman studies (Peercy, 1975*a*,*b*). If it were truly order–disorder, the mode would be a Debye relaxation with a spectral peak at zero frequency, independent of pressure or temperature. Only the width and intensity would depend upon these parameters.

As a final note on KDP, this material exhibits at ambient pressure and zero applied electric field a phase transition that is very slightly discontinuous. Application of modest pressure or field produces a truly continuous transition. That is, the tricritical point is easily accessible [at a critical field of $6\,\mathrm{kV\,cm^{-1}}$, according to Western *et al.* (1978)].

3.1.5.2.11. *Sodium nitrite, $NaNO_2$*

Sodium nitrite exhibits a purely order–disorder transition and has been chosen for discussion to contrast with the systems in the sections above, which are largely displacive. The mechanism of its transition dynamics is remarkably simple and is illustrated in Fig. 3.1.5.19. There is a linear array of Na and N ions. At low temperatures, the arrow-shaped NO_2 ions (within each domain) point in the same direction; whereas above the Curie temperature they point in random directions with no long-range order. The flopping over of an NO_2 ion is a highly nonlinear response. Therefore the response function (spectrum) associated with this NO_2 flip-flop mode will consist of two parts: a high-frequency peak that looks like a conventional phonon response (lightly damped Lorentzian), plus a low-frequency Debye relaxation ('central mode' peaking at zero frequency). Most of the temperature dependence for this mode will be associated with the Debye spectrum. The spectrum of sodium nitrite is shown in Fig. 3.1.5.20.

Particularly interesting is its phase diagram, relating structure(s) to temperature and 'conjugate' field applied along the

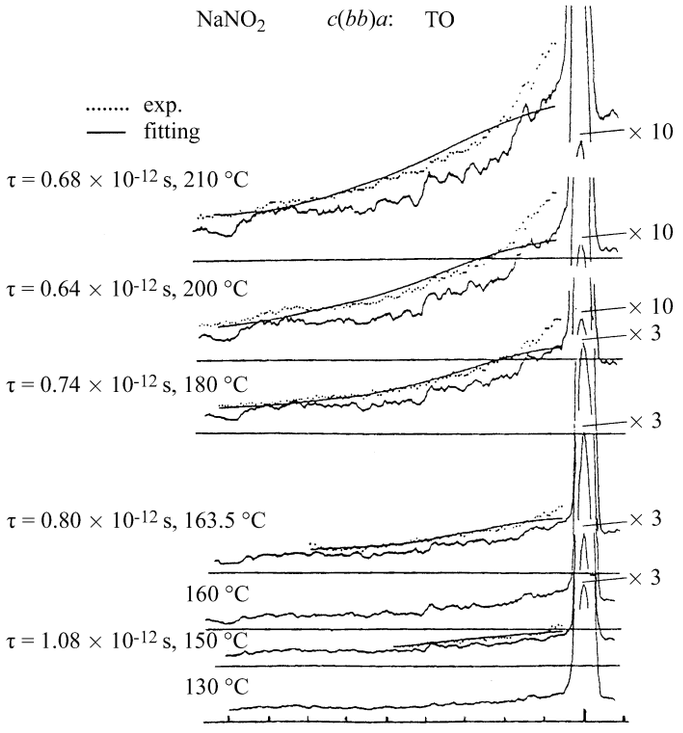

Fig. 3.1.5.20. Raman spectra of sodium nitrite, showing diffusive Debye-like response due to large-amplitude flopping over of nitrite ions [note that the high-frequency phonon-like response is due to the small-amplitude motion of this same normal mode; thus in this system N ions give rise not to $3N$ (non-degenerate) peaks in the spectral response function, but to $3N + 1$].

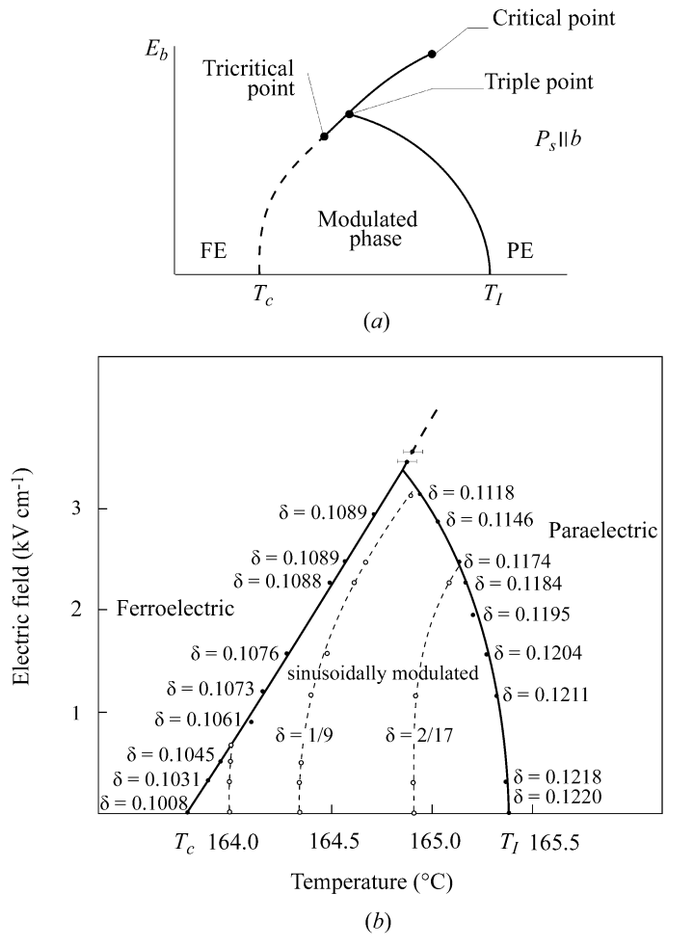

Fig. 3.1.5.21. Phase diagram for sodium nitrite for 'conjugate' electric fields applied along the polar b axis, showing triple point, tricritical point and critical end point. (*a*) Schematic; (*b*) real system.

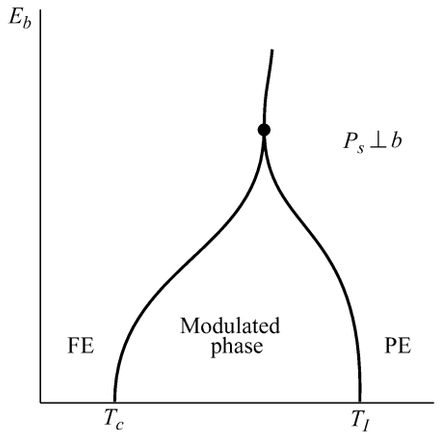

Fig. 3.1.5.22. Phase diagram for sodium nitrite for electric fields applied perpendicular to the polar b axis. In this situation, a Lifshitz point is possible where phase boundaries 'kiss' (touch tangentially).

polar axis. As Fig. 3.1.5.21 illustrates somewhat schematically, there are first-order phase boundaries, second-order phase boundaries, a tricritical point and a critical end point (as in a gas–liquid diagram). If the electric field is applied in a direction orthogonal to the polar axis, a Lifshitz point (Fig. 3.1.5.22) may be expected, in which the phase boundaries intersect tangentially. The ionic conductivity of sodium nitrite has made it difficult to make the figures in Figs. 3.1.5.21 and 3.1.5.22 precise.

3.1.5.2.12. *Fast ion conductors*

As exemplary of this class of materials, we discuss in this section the silver iodide compound $Ag_{13}I_9W_2O_8$. This material has the structure illustrated in Fig. 3.1.5.23. Conduction is *via* transport of silver ions through the channels produced by the W_4O_{16} ions (the coordination is not that of a simple tetrahedrally coordinated WO_4 tungstate lattice).

This crystal undergoes three structural phase transitions (Habbal *et al.*, 1978; Greer *et al.*, 1980; Habbal *et al.*, 1980), as illustrated in Fig. 3.1.5.24. The two at lower temperatures are first-order; that at the highest temperature appears to be perfectly continuous. Geller *et al.* (1980) tried to fit electrical data for this material ignoring the uppermost transition.

As in most of the materials discussed in this review, the phase transitions were most readily observed *via* optical techniques, Raman spectroscopy in particular. The subtle distortions involve oxygen positions primarily and are not particularly well suited to more conventional X-ray techniques. Silver-ion disorder sets in only above the uppermost phase transition, as indicated by the full spectral response (as in the discussion of sodium nitrite in the preceding section).

Infrared (Volkov *et al.*, 1985) and Raman (Shawabkeh & Scott, 1989) spectroscopy have similarly confirmed low-temperature phase transitions in $RbAg_4I_5$ at 44 and 30 K, in addition to the well studied D_3^7–D_3^2 ($R32$–$P321$) transition at 122 K. The two lower-temperature phases increase the size of the primitive cell, but their space groups cannot be determined from available optical data. The 44 K transition is signalled by the abrupt appearance of an intense phonon feature at 12 cm^{-1} in both infrared and Raman spectra.

3.1.5.2.13. *High-temperature superconductors*

It is useful to play Devil's Advocate and point out difficulties with the technique discussed, to indicate where caution might be exercised in its application. $YBa_2Cu_3O_{7-x}$ (YBaCuO) provides such a case. As in the case of $BaMnF_4$ discussed in Section 3.1.5.2.7, there was strong evidence for a structural phase transition near 235 K, first from ultrasonic attenuation (Wang, 1987;

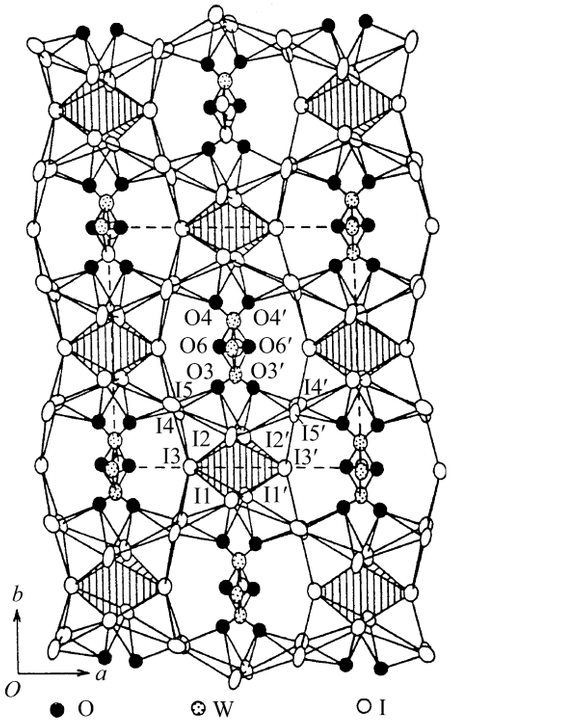

(*a*)

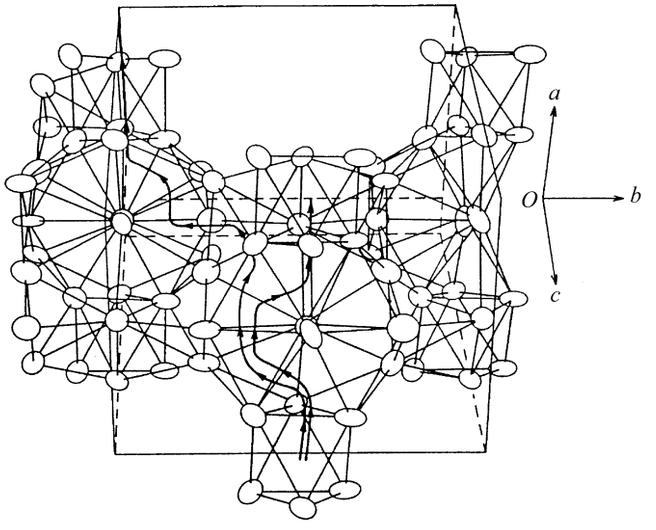

(*b*)

Fig. 3.1.5.23. (*a*) Crystal structure of silver iodide tungstate ($Ag_{13}I_9W_2O_8$); (*b*) showing conduction paths for Ag ions (after Chan & Geller, 1977).

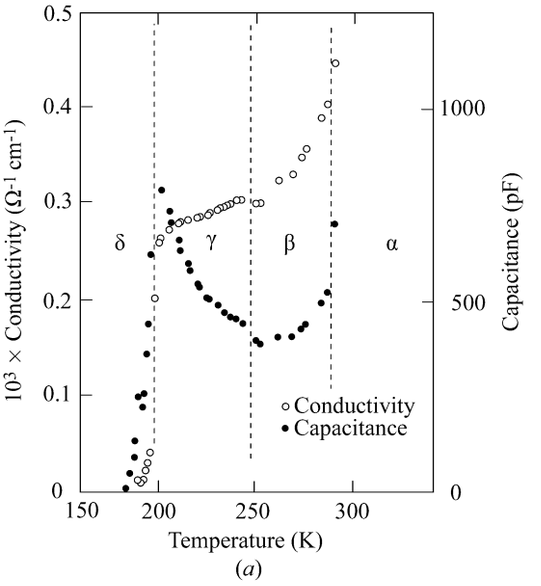

(*a*)

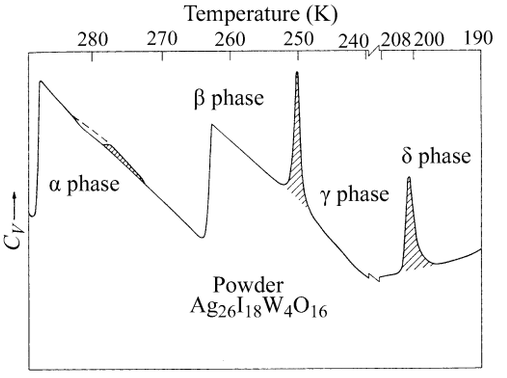

(*b*)

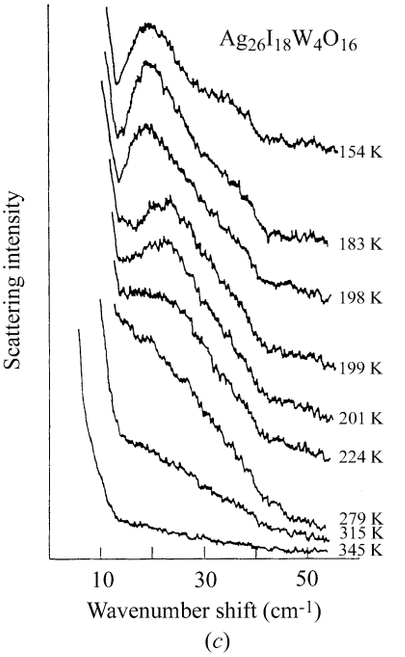

(*c*)

Fig. 3.1.5.24. Evidence for three phase transitions in silver iodide tungstate: (*a*) dielectric and conductivity data; (*b*) specific heat data; (*c*) Raman data. The lower transitions, at 199 and 250 K, are first order; the upper one, at 285 K, is second order.

Laegreid *et al.*, 1987) and then from Raman studies (Zhang *et al.*, 1988; Huang *et al.*, 1987; Rebane *et al.*, 1988). However, as years passed this was never verified *via* neutron or X-ray scattering. Researchers questioned (MacFarlane *et al.*, 1987) whether indeed a phase transition exists at such a temperature in this important material. At present it is a controversial and occasionally contentious issue. A difficulty is that light scattering in metals probes only the surface. No information is obtained on the bulk. Ultrasonic attenuation and internal friction probe the bulk, but give scanty information on mechanisms or structure.

In the specific case of YBaCuO, the 'extra' phonon line (Fig. 3.1.5.25) that emerges below 235 K is now known not to be from the superconducting $YBa_2Cu_3O_{7-x}$ material; its frequency of 644 cm^{-1} is higher than that of any bulk phonons in that material. However, this frequency closely matches that of the highest

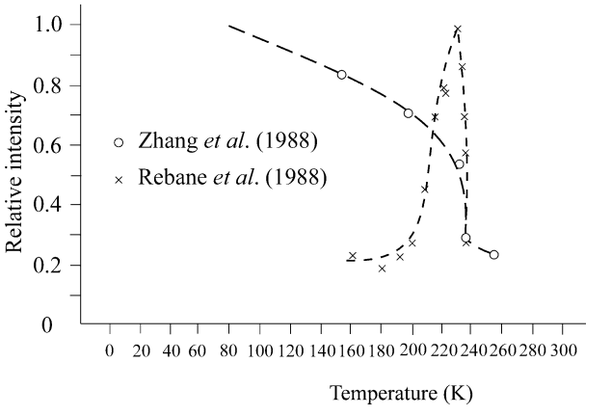

Fig. 3.1.5.25. Raman spectra of $YBa_2Cu_3O_{7-x}$ below an apparent phase transition at *ca.* 235 K (Zhang *et al.*, 1988).

LO (longitudinal optical) phonon in the semiconducting $YBa_2Cu_3O_{6+x}$ material, suggesting that the supposed phase transition at 235 K may be not a structural transition but instead a chemical transition in which oxygen is lost or gained at the surface with temperature cycling.

3.1.5.3. *Low-temperature ferroelectric transitions*

It has historically been difficult to establish the nature of ferroelectric phase transitions at cryogenic temperatures. This is simply because the coercive fields for most crystals rise as the temperature is lowered, often becoming greater than the breakdown fields below *ca.* 100 K. As a result, it is difficult to demonstrate *via* traditional macroscopic engineering techniques (switching) that a material is really ferroelectric. Some authors have proposed (*e.g.* Tokunaga, 1987) on theoretical grounds the remarkable (and erroneous) conjecture that no crystals have Curie temperatures much below 100 K. A rebuttal of this speculation is given in Table 3.1.5.1 in the form of a list of counter-examples. References may be found in the 1990 Landolt–Börnstein Encyclopedia of Physics (Vol. 28a). The original work on pure cadmium titanate and on lead pyrochlore (Hulm, 1950, 1953) did not demonstrate switching, but on the basis of more recent studies on mixed crystals $Ca_{2-2x}Pb_{2x}Nb_2O_7$ and $Ca_xCd_{1-x}TiO_3$, it is clear that the pure crystals are ferroelectric at and below the stated temperatures.

Hence, in Table 3.1.5.1 we see examples where X-ray structural studies may establish the symmetries requisite for ferroelectricity without the macroscopic switching being demonstrated. This is the converse case to that primarily emphasized in this section (*i.e.* the use of techniques complementary to X-ray scattering to determine exact crystal symmetries); it is useful to see these reverse cases to demonstrate the full complementarity of X-ray crystallography and dynamic spectroscopic techniques.

Table 3.1.5.1. *Low-temperature ferroelectrics*

Formula	Curie temperature T_c (K)	Curie constant C (K)	Entropy change ΔS (cal mol^{-1} K^{-1})
$NH_4Al(SO_4)_2{\cdot}12H_2O$	71	?	?
$NH_4Fe(SO_4)_2{\cdot}12H_2O$	88	400	0.15
$(NH_4)_2Cd(SO_4)_3$	95	?	?
$CdTiO_3$	55	4.5×10^4	?
$Pb_2Nb_2O_7$	15.3	?	?
$LiTlC_4H_4O_6{\cdot}H_2O$	10.5	?	?
$K_3Li_2Nb_5O_{15}$	7	?	?

3.1.6. Group informatics and tensor calculus

By V. Kopský and P. Boček

We shall briefly describe here the intentions and contents of the accompanying software package *GI⋆KoBo*-1 (*Group Informatics*, first two letters of authors names, release 1). A more detailed description is contained in the manual; the user may consult this file on the screen, but we recommend that it is printed out and that the printout is followed in order to become familiar with the theoretical background as well as with more detailed instructions for the use of the software.

The main purpose of this software is to describe the changes of tensor properties of crystalline materials during ferroic phase transitions, including basic information about domain states. The software provides powerful information in a standardized manner and it is based on a few advanced methodical points that are not yet available in textbooks. These points are:

(i) The introduction of *typical variables*, which was inspired by the *symbolic method* of the old invariant theory (Weitzenböck, 1923).

(ii) The method of Clebsch–Gordan products (Kopský, 1976*a*,*b*). The name stems from Clebsch–Gordan coefficients, known in quantum mechanics as coefficients of momentum addition. In this case, the coefficients are connected with the orthogonal group $\mathcal{O}(3)$; analogous coefficients were later introduced and calculated for crystal point groups (Koster *et al.*, 1963). They appear in Clebsch–Gordan products, which represent a better adaptation of results for our purposes.

(iii) Tables of *tensorial covariants* (Kopský, 1979*a*,*b*). The name covariant may sound rather unusual now, but it was originally used by Weyl (1946); it is equivalent to *symmetry-adapted bases* (*form-invariant bases* and other terms are also used). The term covariant is classical and its semantical use is easier.

(iv) Tables of *fine structures of domain states* (Kopský, 1982). These are contained in a booklet which is practically unknown though, together with tables of tensorial covariants, it contains all answers concerning changes of tensor properties at ferroic phase transitions.

Remark. The original term *fine domain structure* was amended because it is not quite accurate.

(v) *Extended integrity bases* (Patera *et al.*, 1978; Kopský, 1979*c*). These represent finite sets of polynomial invariants and covariants suitable for the calculation of all types of interactions in symmetric systems.

(vi) *Lattices of subgroups* (Ascher, 1968; Kopský, 1982). Subgroups of a group constitute a partially ordered set of special properties called a *lattice*. The unfortunate coincidence of the term (in English) with crystallographic lattices should be disregarded; it is always possible to see from the context what we mean by this term.

These methods provide good ammunition for all types of group-theoretical considerations where work with characters is insufficient and knowledge of the explicit bases of irreducible representations is necessary. This is exactly the case for the theory of structural phase transitions, and the consideration of domain states, pairs of domain states and domain walls or twin boundaries. The main results of the software are contained in tables of symmetry descents $G \Downarrow H$ and/or $G \Downarrow F_i$, where G is the parent point group, H its normal subgroup and F_i is the set of conjugate subgroups. These tables provide information about changes of tensors at ferroic phase transitions as well as basic information about interactions, and they are also supplemented by tables of equitranslational subgroups of space groups.

To make this exposition quite clear, we begin in the manual from the beginning with a brief review of elementary group-theoretical concepts used in the software. Relevant elementary tables (listed below in Section A) are followed by more advanced information proceeding towards the central goal of providing information for all symmetry descents (Section B). To achieve this goal, it was also necessary to introduce our own standard